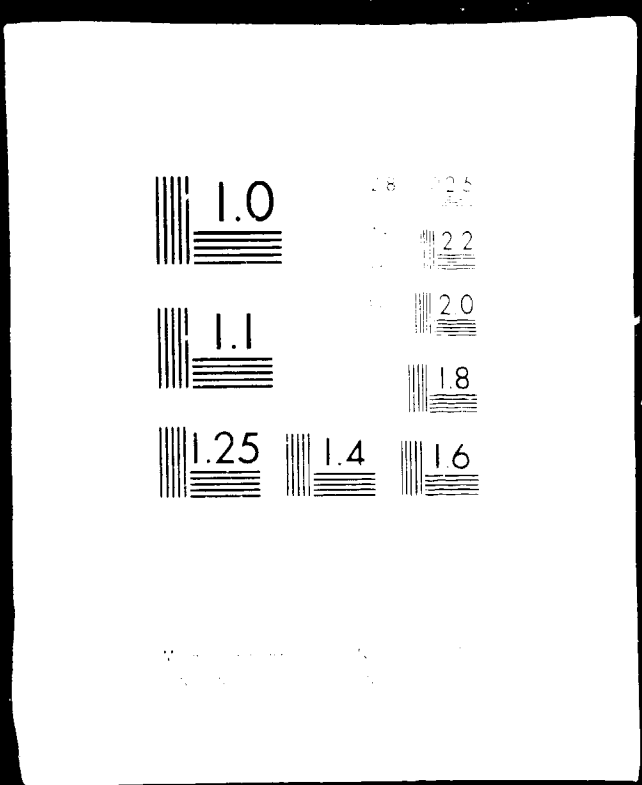

CR-152010

SIMULATION OF A SYNERGISTIC SIX-POST MOTION SYSTEM ON THE FLIGHT SIMULATOR FOR ADVANCED AIRCRAFT AT NASA-AMES

By

Samiresh C. Bose

and

Benton L. Parris

JULY 1977

Prepared under Contract
No. NAS2-7806 by
COMPUTER SCIENCES CORPORATION
Mountain View, California

for

NATIONAL AERONAUTICS AND
SPACE ADMINISTRATION

Ames Research Center
Moffett Field, California 94035

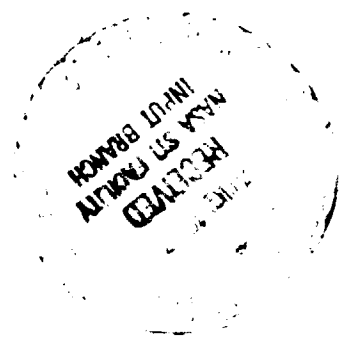

TABLE OF CONTENTS

LIST OF SYMBOLS

$\bar{A}_i$ - Vector position of the upper attach point of actuator i with respect to the origin of the moving reference frame expressed in the fixed frame coordinates

$\bar{A}_{i,m}$ - Vector $\bar{A}_i$ expressed in moving frame coordinates

$A^x_{i,m}, A^y_{i,m}, A^z_{i,m}$ - Components of $\bar{A}_{i,m}$

a_ℓ - Generalized acceleration limit

$\bar{B}_i$ - Vector position of the lower attach point of actuator i with respect to the origin of the fixed reference frame expressed in the fixed frame coordinates

B^x_i, B^y_i, B^z_i - Components of $\bar{B}_i$

E_j, G_j - Components of the length equation for actuator j which are independent of the simulator position component x_s

I - Identity matrix

$\bar{i}_m, \bar{j}_m, \bar{k}_m$ - Right-handed triad of unit vectors in the moving reference frame

$\bar{i}_o, \bar{j}_o, \bar{k}_o$ - Right-handed triad of unit vectors in the fixed reference frame

$\bar{i}_s, \bar{j}_s, \bar{k}_s$ - Left-handed triad of unit vectors in the simulator reference frame

$\bar{\ell}_i$ - Vector in fixed reference frame from lower attach point to upper attach point of actuator i

$\ell_i^x, \ell_i^y, \ell_i^z$ - Components of $\bar{\ell}_i$

p_ℓ - Generalized position limit

$\bar{R}$ - Vector in the fixed reference from the origin of the fixed reference frame to the origin of the moving reference frame

R^x, R^y, R^z - Components of $\bar{R}$

$\bar{r}_i$ - Vector in the fixed reference frame from the origin of the fixed reference frame to the upper attach point of actuator i

$\bar{s}$ - Vector in the simulator reference frame from the origin of the simulator reference frame to the origin of the moving reference frame

T - Euler angle transformation matrix to transform coordinates in the moving frame to coordinates in the fixed frame

T_{ij} - Elements of T; i=1,2,3 and j=1,2,3

v_ℓ - Generalized velocity limit

x - Generalized coordinate

x_m, y_m, z_m - Moving frame coordinates

x_o, y_o, z_o - Fixed frame coordinates

x_s, y_s, z_s - Simulator coordinates

x_ℓ, y_ℓ, z_ℓ - Position limits in simulator coordinates

z^* - Neutral position of the origin of the simulator frame with respect to the fixed frame

ψ, θ, ϕ - Euler angle orientation of the moving frame with respect to the fixed frame

$\S_x, \S_y, \S_z$ - Components of $\bar{\S}$

$\bar{\S}$ - Generalized vector

$\S$ - Generalized variable of integration for generalized coordinate x

$| \, |$ - Denotes the magnitude of a vector

Subscripts:

m - Moving reference frame

o - Fixed reference frame

s - Simulator reference frame

Superscripts:

T - Transpose

x - x component of a vector

y - y component of a vector

z - z component of a vector

A bar over a symbol denotes a vector

A dot over a symbol denotes a derivative with respect to time

SUMMARY

Motion system drive philosophy and corresponding real-time software have been developed for the purpose of simulating the characteristics of a typical synergistic Six-Post Motion System (SPMS) on the Flight Simulator for Advanced Aircraft (FSAA) at NASA-Ames which is a non-synergistic motion system. This paper gives a brief description of these two types of motion systems and the general method of producing motion cues on the FSAA. An actuator extension transformation which allows the simulation of a typical SPMS by appropriate drive washout and variable position limiting is described.

1.0 INTRODUCTION

The use of a moving-base flight simulator to supply motion cues to the pilot requires an organized scheme of coordination, washout, and limiting of drive commands to produce realistic cues while remaining within the physical constraints of the motion system. The motion drive software for both the SPMS at NASA-Langley and the FSAA at NASA-Ames is based on the general techniques developed by Schmidt and Conrad [1 and 2]. However, the design of the software for these two motion systems is highly dependent on the specific system's characteristics.

A more involved problem is that of developing a scheme for producing motion commands to the FSAA resulting in motion cues similar to those produced by a typical synergistic SPMS. Such a scheme was required for the purpose of evaluating different motion systems during a joint NASA/ USAF experiment recently conducted at Ames.

This paper includes a discussion of the characteristics of a typical synergistic SPMS and the non-synergistic FSAA. The motion drive software for the FSAA is reviewed and the scheme for simulating a typical SPMS on the FSAA is presented in detail.

2.0 DESCRIPTION OF MOTION SYSTEMS

All moving-base aircraft simulators possess position, velocity, and acceleration constraints which prevent them from exactly reproducing the full motion histories of an aircraft. These constraints vary with the number of degrees of freedom and performance limitations of any specific motion system design.

The FSAA at NASA-Ames consists of a transport-type cab integrated into a system of drive mechanisms such as electrical motor/generator combinations, drive belts, timing chains, and gears which form a six-degree-of-freedom motion system [3]. A photograph of this system is shown in Figure 1. Although a detailed exposition of the performance capability of the FSAA is not presented in this paper, a summary of this capability is given in Table 1. The FSAA is capable of motion in each axis independent of the other axes (i.e., a non-synergistic system). The current FSAA drive technique incorporates a velocity command scheme with position, velocity, and acceleration sensors supplying feedback to the software or the motion monitoring system. The most unique feature of the FSAA is its ± 40. feet of lateral travel capability.

A typical SPMS consists of a cab mounted on a platform which is driven by six servomechanisms utilizing hydraulically powered actuators or legs. A photograph of such a system (the one at NASA-Langley) is shown in Figure 2. A schematic representation of the actuator geometry for this system is given in Figure 3. The points where the actuators connect to the moving platform form an equilateral triangle and the actuators have a minimum length of 8.60 feet (2.62 m) and a maximum length of 13.58 feet (4.14 m). When all six actuators are at their neutral position (midway between minimum and maximum extension) the platform achieves a neutral height (Z*) of 8.33 feet (2.54 m). This actuator geometry and the performance capability presented in Table 2 (not exactly the capability of the NASA-Langley system) were considered to be typical for the SPMS model used later in this development. A

typical SPMS does not have drive systems for each degreee-of-freedom but achieves motion in all six degrees by a combination of actuator extensions (i.e., a synergistic system). The transformation which converts simulator position information to leg extensions for this type of system is discussed in detail in this paper (Section 4.0).

3.0 MOTION SYSTEM DRIVE PHILOSOPHY FOR THE FLIGHT SIMULATOR FOR ADVANCED AIRCRAFT (FSAA)

Designing the drive logic for any motion system involves establishment of a scheme by which motion cues are transmitted to the pilot while keeping the movement of the simulator within its constraints. After a motion cue has been transmitted, the motion system should return to its neutral position without the pilot being aware of this movement. The resultant tendency to keep the simulator near its neutral position maximizes the allowable motion for subsequent cues.

The motion system drive philosophy for the FSAA involves producing coordinated motion cues by generating high frequency translational and rotational accelerations supplemented by low frequency forward and side forces via proper cab rotation (i.e., orientation of the pilot within the gravitational field). The latter technique is commonly referred to as "residual tilt". The major conjecture in this philosophy is that very low frequency accelerations are not sensed and/or are not important to the pilot with respect to motion cue adequacy for most tasks of interest. Other factors involved in the drive philosophy are discussed in detail in [4].

A simplified schematic description of a typical simulation configuration on the FSAA is shown in Figure 4 and a conceptual block diagram of the motion system drive logic is presented in Figure 5. This diagram presents the relationship between longitudinal translation and pitch motion or the relationship between lateral translation and roll motion, since these motion pairs are coupled in the same manner. The vertical translation and yaw motion of the simulator are treated independently. There is no "residual tilt" term for the yaw axis and no compensation in the vertical axis due to high frequency yaw rotations.

For the translational axes the pilot station accelerations are scaled and passed through second order high pass filters. High frequency translational acceleration components are then integrated to obtain washed out

translational velocity components. Similarly, rotational velocities are obtained in roll, pitch, and yaw. The rotational velocities, however, are still in the aircraft body axes. Gimble angle transformation from aircraft body axes to simulator cab axes produces simulator drive rotational velocity commands. These rotational rate commands are modified by "residual tilt" terms computed from low frequency translational accelerations. In order to give the effect of coordinated motion cues the forward and side forces resulting from washed out high frequency rotational rates are subtracted from the high frequency translational cues. The final translational rate commands are transformed from aircraft body axes to simulator cab axes. Both the translational and rotational velocity commands are software limited. To keep the simulator from drifting, position feedback is used to compensate the outgoing velocity commands to the simulator.

4.0 ACUTATOR EXTENSION TRANSFORMATION FOR THE SYNERGISTIC SIX-POST MOTION SYSTEM (SPMS)

To obtain actuator lengths from a given platform centroid position a transformation is required. This transformation [5] transforms a given vector of three translational positions and three rotational orientations into six leg lengths of the six actuators.

The base platform and the moving platform are shown in Figure 6. Consider each platform of the six-legged motion system to have an associated coordinate system as shown in Figure 6. The fixed reference frame (x_o, y_o, z_o) has its origin at the centroid of the fixed platform and the moving reference frame (x_m, y_m, z_m) has its origin at the centroid of the moving platform. The two reference frames are both right-handed coordinate systems and their axes are aligned when the moving platform is at its neutral position. For any actuator (i) the vector relationships between the two reference frames are illustrated in Figure 7 and can be expressed as

$$\begin{aligned} \bar{r}_i &= \bar{B}_i + \bar{\ell}_i \\ \bar{r}_i &= \bar{A}_i + \bar{R} \end{aligned} \qquad (1) \qquad i = 1,\ldots,6$$

which yields

$$\bar{\ell}_i = \bar{A}_i - \bar{B}_i + \bar{R} \qquad (2)$$

A graphical representation of these vectors for all six actuators is presented in Figure 8.

Equation (2) gives the orientation and length of each actuator as a function of the dimensions of the fixed and moving (or payload) platform and the orientation of the moving platform with respect to the fixed platform. Equation (2) is expressed strictly in the fixed platform reference frame. Hence, the vector $\bar{B}_i$ is known from the dimensions and leg attachment geometry of the fixed platform (Table 3). However, the vectors $\bar{A}_i$ and $\bar{R}$ are yet to be determined.

If we define $(\bar{i}_o, \bar{j}_o, \bar{k}_o)$ as the triad of unit vectors in the fixed platform reference frame, we can represent $\bar{\ell}_i$, $\bar{A}_i$, $\bar{B}_i$ and $\bar{R}$ as

$$\left.\begin{aligned} \bar{\ell}_i &= \ell_i^x\,\bar{i}_o + \ell_i^y\,\bar{j}_o + \ell_i^z\,\bar{k}_o \\ \bar{A}_i &= A_i^x\,\bar{i}_o + A_i^y\,\bar{j}_o + A_i^z\,\bar{k}_o \\ \bar{B}_i &= B_i^x\,\bar{i}_o + B_i^y\,\bar{j}_o + B_i^z\,\bar{k}_o \\ \bar{R} &= R^x\,\bar{i}_o + R^y\,\bar{j}_o + R^z\,\bar{k}_o \end{aligned}\right\} \quad (3)$$

It will be shown later that the components (R^x, R^y, R^z) can all be expressed in terms of simulator coordinates (x_s, y_s, z_s).

Defining $(\bar{i}_m, \bar{j}_m, \bar{k}_m)$ as the triad of unit vectors in the moving platform reference frame and (ψ, θ, ϕ) as the ordered rotation in yaw, pitch, and roll of the moving frame with respect to the neutral position in which the moving and fixed frames are aligned (i.e., the moving axes are parallel to the fixed axes), the relation between the two reference frames is given by

$$\begin{bmatrix} \bar{i}_o \\ \bar{j}_o \\ \bar{k}_o \end{bmatrix} = [T] \begin{bmatrix} \bar{i}_m \\ \bar{j}_m \\ \bar{k}_m \end{bmatrix} \quad (4)$$

where [T] is the Euler angle transformation matrix and is expressed as

$$[T] = \begin{bmatrix} T_{11} & T_{12} & T_{13} \\ T_{21} & T_{22} & T_{23} \\ T_{31} & T_{32} & T_{33} \end{bmatrix} \quad (5)$$

and

$$\left.\begin{aligned} T_{11} &= \cos\psi\cos\theta & T_{12} &= \cos\psi\sin\theta\sin\phi - \sin\psi\cos\phi & T_{13} &= \cos\psi\sin\theta\cos\phi + \sin\psi\sin\phi \\ T_{21} &= \sin\psi\cos\theta & T_{22} &= \sin\psi\sin\theta\sin\phi + \cos\psi\cos\phi & T_{23} &= \sin\psi\sin\theta\cos\phi - \cos\psi\sin\phi \\ T_{31} &= -\sin\theta & T_{32} &= \cos\theta\sin\phi & T_{33} &= \cos\theta\cos\phi \end{aligned}\right\} \quad (6)$$

The vector from the centroid of the moving platform to the attach point of any actuator (i) can be expressed in the moving frame as

$$\bar{A}_{i,m} = A^x_{i,m}\bar{i}_m + A^y_{i,m}\bar{j}_m + A^z_{i,m}\bar{k}_m \qquad i=1,\ldots,6 \qquad (7)$$

where the components $(A^x_{i,m}, A^y_{i,m}, A^z_{i,m})$ are known from the geometry of the moving platform (Table 3). The $\bar{A}_i$ vectors in the fixed frame are then given by

$$\bar{A}_i = [T]\,\bar{A}_{i,m} \qquad i=1,\ldots,6 \qquad (8)$$

and equation (2) can now be written as

$$\bar{\ell}_i = [T]\,\bar{A}_{i,m} - \bar{B}_i + \bar{R} \qquad (9)$$

To obtain the scalar form of the actuator extension transformation given by equation (9) we multiply $\bar{\ell}_i$ by its transpose $\bar{\ell}_i^T$ giving

$$\begin{aligned} \bar{\ell}_i^T\,\bar{\ell}_i &= \{[T]\,\bar{A}_{i,m} - \bar{B}_i + \bar{R}\}^T\,\{[T]\,\bar{A}_{i,m} - \bar{B}_i + \bar{R}\} \\ &= \{\bar{A}^T_{i,m}[T]^T - \bar{B}_i^T + \bar{R}^T\}\,\{[T]\,\bar{A}_{i,m} - \bar{B}_i + \bar{R}\} \\ &= \bar{A}^T_{i,m}[T]^T[T]\,\bar{A}_{i,m} - \bar{A}^T_{i,m}[T]^T\bar{B}_i + \bar{A}^T_{i,m}[T]^T\bar{R} - \bar{B}_i^T[T]\,\bar{A}_{i,m} + \bar{B}_i^T\bar{B}_i \\ &\quad - \bar{B}_i^T\bar{R}\,\bar{R}^T[T]\,\bar{A}_{i,m} - \bar{R}^T\bar{B}_i + \bar{R}^T\bar{R} \end{aligned}$$

$$\bar{\ell}_i^T \bar{\ell}_i = |\bar{A}_{i,m}|^2 - \bar{A}_{i,m}^T[T]^T\bar{B}_i + \bar{A}_{i,m}^T[T]^T\bar{R} - \bar{B}_i^T[T]\,\bar{A}_{i,m} + |\bar{B}_i|^2 - \bar{B}_i^T\bar{R} + \bar{R}^T[T]\,\bar{A}_{i,m}$$

$$- \bar{R}^T\bar{B}_i + |\bar{R}|^2 \tag{10}$$

where we have used the fact that for Euler angle transformation

$$[T]^T[T] = I \tag{11}$$

and I is the identity matrix.

Using the general definition

$$\bar{\varsigma}^T\bar{\varsigma} = |\bar{\varsigma}| = \sqrt{\varsigma_x^2 + \varsigma_y^2 + \varsigma_z^2} \tag{12}$$

Equation (10) can be written as

$$|\bar{\ell}_i|^2 = \bar{\ell}_i^T \bar{\ell}_i$$

$$= (A^x_{i,m})^2+(A^y_{i,m})^2+(A^z_{i,m})^2+(B^x_i)^2+(B^y_i)^2+(B^z_i)^2$$

$$-\begin{bmatrix} A^x_{i,m} & A^y_{i,m} & A^z_{i,m} \end{bmatrix} \begin{bmatrix} T_{11} & T_{21} & T_{31} \\ T_{12} & T_{22} & T_{32} \\ T_{13} & T_{23} & T_{33} \end{bmatrix} \begin{bmatrix} B^x_i \\ B^y_i \\ B^z_i \end{bmatrix}$$

$$+\begin{bmatrix} A^x_{i,m} & A^y_{i,m} & A^z_{i,m} \end{bmatrix} \begin{bmatrix} T_{11} & T_{21} & T_{31} \\ T_{12} & T_{22} & T_{32} \\ T_{13} & T_{23} & T_{33} \end{bmatrix} \begin{bmatrix} R^x \\ R^y \\ R^z \end{bmatrix}$$

$$-\begin{bmatrix} B^x_i & B^y_i & B^z_i \end{bmatrix} \begin{bmatrix} T_{11} & T_{12} & T_{13} \\ T_{21} & T_{22} & T_{23} \\ T_{31} & T_{32} & T_{33} \end{bmatrix} \begin{bmatrix} A^x_{i,m} \\ A^y_{i,m} \\ A^z_{i,m} \end{bmatrix}$$

$$-\begin{bmatrix} B^x_i & B^y_i & B^z_i \end{bmatrix} \begin{bmatrix} R^x \\ R^y \\ R^z \end{bmatrix} -\begin{bmatrix} R^x & R^y & R^z \end{bmatrix} \begin{bmatrix} B^x_i \\ B^y_i \\ B^z_i \end{bmatrix}$$

$$+\begin{bmatrix} R^x & R^y & R^z \end{bmatrix} \begin{bmatrix} T_{11} & T_{12} & T_{13} \\ T_{21} & T_{22} & T_{23} \\ T_{31} & T_{32} & T_{33} \end{bmatrix} \begin{bmatrix} A^x_{i,m} \\ A^y_{i,m} \\ A^z_{i,m} \end{bmatrix}$$

$$+(R^x)^2+(R^y)^2+(R^z)^2 \qquad (13)$$

Equation (13) can be simplified to yield

$$
\begin{aligned}
|\bar{\ell}_i|^2 = {} & (R^x)^2+2R^x(A^x_{i,m}T_{11}+A^y_{i,m}T_{12}+A^z_{i,m}T_B-B^x_i) \\
& +(R^y)^2+2R^y(A^x_{i,m}T_{21}+A^y_{i,m}T_{22}+A^z_{i,m}T_{23}-B^y_i) \\
& +(R^z)^2+2R^z(A^x_{i,m}T_{31}+A^y_{i,m}T_{32}+A^z_{i,m}T_{33}-B^z_i) \\
& +(A^x_{i,m})^2+(A^y_{i,m})^2+(A^z_{i,m})^2+(B^x_i)^2+(B^y_i)^2+(B^z_i)^2 \\
& -2B^x_i(A^x_{i,m}T_{11}+A^y_{i,m}T_{12}+A^z_{i,m}T_{13}) \\
& -2B^x_i(A^x_{i,m}T_{21}+A^y_{i,m}T_{22}+A^z_{i,m}T_{23}) \\
& -2B^z_i(A^x_{i,m}T_{31}+A^y_{i,m}T_{32}+A^z_{i,m}T_{33})
\end{aligned}
\tag{14}
$$

Equation (14) is still in terms of R^x, R^y and R^z. These quantities are still unknown and need to be related to the translational position of the simulator. In order to do this a transformation between the centroid of the moving platform of the motion base at its neutral height and the origin of the linear position follow-up measuring potentiometers is necessary. The coordinate system ($\bar{i}_s$, $\bar{j}_s$, $\bar{k}_s$) to measure the position of the simulator for the FSAA is a left handed coordinate system whereas the coordinate system ($\bar{i}_o$, $\bar{j}_o$, $\bar{k}_o$) and ($\bar{i}_m$, $\bar{j}_m$, $\bar{k}_m$) are right handed coordinate systems.

The different coordinate systems are shown in Figure 9. For any arbitrary position of the simulator given by $\bar{S}$ defined as

$$\bar{S} = x_s\bar{i}_s+y_s\bar{j}_s+z_s\bar{k}_s \tag{15}$$

the relationship between the components of the vectors $\bar{R}$ and $\bar{S}$ are given as

$$\left.\begin{aligned} R^x &= x_s \\ R^y &= y_s \\ \text{and} \quad R^z &= -(z_s + z^*) \end{aligned}\right\} \tag{16}$$

where z^* = neutral height = 8.33 feet

5.0 DRIVE PHILOSOPHY FOR SIMULATING AN SPMS ON THE FSAA

The drive philosophy adopted for simulating a typical SPMS on the FSAA was to preserve the general structure of the FSAA philosophy (Figure 5) as much as possible but to incorporate the synergistic effects of an SPMS by variable position limiting. This philosophy is somewhat different than one that might be used for designing drive logic for a real SPMS. An example of a real SPMS philosophy can be found in Reference 6.

A conceptual block diagram of the scheme developed for simulating an SPMS is presented in Figure 10.

The current position of the FSAA is given by the vector (x_s, y_s, z_s, ϕ, θ, ψ) at any instant of time as measured by the linear and rotational position follow-up potentiometers. Conceptually, had there actually been a six-actuator system the position vector (x_s, y_s, z_s, ϕ, θ, ψ) would have resulted from a certain specific combination of six-actuator lengths. Hence, the measured position (x_s, y_s, z_s, ϕ, θ, ψ) is used in the actuator transformation equation given by equation (14) to determine the six-actuator lengths. The actuator transformation equation requires the six-actuator motion base dimensions ($\bar{A}_{i,m}$,$\bar{B}_i$), components of the Euler angle transformation [T], and the coordinate transformation between the vectors $\bar{R}$ and $\bar{S}$ (equation (16)). These computations are done prior to using the actuator transformation equation as shown in Figure 10. The s ' actuator lengths are then compared with each other and using the longest and the shortest actuators a prediction is made of the translational position limits (x_ℓ, y_ℓ, z_ℓ) based on current position of the simulator. For the rotational axes, fixed angular excursion limits are used. These six limits restrict the subsequent motion cue that can be transmitted to the pilot. The details of the method of predicting the position limits are given in Appendix A. The desired position commands from the FSAA washout scheme are then compared to the six position limits. Based on this comparison the objective is to compute velocity limits. As shown in Figure 10 if a position limit is exceeded then the velocity limit is set equal to zero.

Otherwise, a position-velocity parabolic limiting is performed. This parabolic limiting scheme is discussed in detail in Appendix B. The desired velocity command as obtained from the FSAA motion washout is then limited to the computed velocity limit. As a final limiting, this limited velocity is compared with the past velocity command to predict the resulting acceleration. The final velocity command is then limited to produce accelerations within the lower acceleration capability of the two motion bases. The outgoing velocity is then compensated to prevent the simulator from drifting.

6.0 CONCLUDING REMARKS

This report has presented a technique of modeling synergistic motion simulation on a non-synergistic motion simulator. Such motion simulation software can also be used for simulation of different types of actuator driven motion simulators for evaluation, testing and research purposes.

The report has discussed and compared the characteristics of a synergistic actuator driven motion base and the FSAA which has a non-synergistic independent axis driven system. The general problem of the motion drive logic design has been discussed and the washout scheme for the FSAA has been outlined. The limitations and the restrictions of an actuator driven motion base have been incorporated into the motion drive scheme of the FSAA.

This did not require major modifications to the FSAA washout scheme. In particular, an actuator extension transformation is required but no iterative inverse transformation is required.

Integrating this drive scheme within a recent KC-135 aircraft simulation required some modification to the washout characteristics in order to match the SPMS limiting envelope. However, the general opinion was that the simulated SPMS gave the effect of an actuator driven motion system.

It should be noted that only synergistic systems with performance capability within that of the FSAA can be simulated with this scheme.

APPENDIX A

METHOD FOR PREDICTING SPMS POSITION LIMITS

It has been shown that the lengths of the actuators $|\bar{\ell}_i|$ for a given position (x_s, y_s, z_s, ϕ, θ, ψ) of the moving platform portion of a typical SPMS with actuator attachment geometry $\bar{A}_{i,m}$ and $\bar{B}_i$ can be expressed as

$$
\begin{aligned}
|\bar{\ell}_i|^2 = {} & x_s^2+2x_s(A^x_{i,m}T_{11}+A^y_{i,m}T_{12}+A^z_{i,m}T_{13}-B^x_i) \\
& +y_s^2+2y_s(A^x_{i,m}T_{21}+A^y_{i,m}T_{22}+A^z_{i,m}T_{23}-B^y_i) \\
& +(z_s+z^*)^2-2(z_s+z^*)(A^x_{i,m}T_{31}+A^y_{i,m}T_{32}+A^z_{i,m}T_{33}-B^z_i) \\
& +(A^x_{i,m})^2+(A^y_{i,m})^2+(A^z_{i,m})^2+(B^x_i)^2+(B^y_i)^2+(B^z_i)^2 \\
& -2B^x_i(A^x_{i,m}T_{11}+A^y_{i,m}T_{12}+A^z_{i,m}T_{13}) \\
& -2B^y_i(A^x_{i,m}T_{21}+A^y_{i,m}T_{22}+A^z_{i,m}T_{23}) \\
& -2B^z_i(A^x_{i,m}T_{31}+A^y_{i,m}T_{32}+A^z_{i,m}T_{33}) \qquad \text{(A1)} \\
& i = 1,\ldots,6
\end{aligned}
$$

These lengths can be used to predict the remaining travel which is crucial in the determination of maximum motion cue generation capability of the SPMS under consideration.

The displacement of a typical SPMS in any one degree-of-freedom alters the maximum displacement that may then be achieved individually in each of the remaining five degrees-of-freedom. Since there can be almost an infinite number of possible combinations of the six displacements for this type of system, there exist an equally large number of position limits. Hence, the set of position limits of an SPMS is not fixed and must be determined for each set of displacements.

The following technique for predicting the position limits of an SPMS is similar to the one used at NASA-Langley on their synergistic motion base [6]. This technique assumes that the most strict constraint on travel, at any instant of time, is governed by the position of the shortest and longest actuator at that instant.

Having obtained the current six actuator lengths using equation (A1), the maximum and minimum length actuators can be identified. The current position limit for each axis is then determined by fixing the other five displacements at their current values and choosing the value of the displacement under consideration that is the minimum of (1) the value specified as an absolute limit, (2) the value which would produce maximum extension of the longest actuator, or (3) the value which would produce maximum contraction of the shortest actuator.

As an example, consider the prediction of the current position limit for x_s. From equation (A1) we determine j such that

$$|\bar{\ell}_j| \geq |\bar{\ell}_i| \quad , \quad i = 1,\ldots,6 \tag{A2}$$

substituting $|\bar{\ell}_j|$ for $|\bar{\ell}_i|$ in equation (A1) we obtain

$$|\bar{\ell}_j|^2 = x_s^2 + 2x_s G_j + E_j \tag{A3}$$

where G_j and E_j are dependent on the other five degrees-of-freedom (y_s, z_s, ϕ, θ, ψ) at that instant and can be expressed as

$$G_j = A^x_{j,m} T_{11} + A^y_{j,m} T_{12} + A^z_{j,m} T_{13} - B^x_j \tag{A4}$$

and $$E_j = y_s^2+2y_s(A^x_{j,m}T_{21}+A^y_{j,m}T_{22}+A^z_{j,m}T_{23}-B^y_j)$$

$$+(z_s+z^*)^2-2(z_s+z^*)(A^x_{j,m}T_{31}+A^y_{j,m}T_{32}+A^z_{j,m}T_{33}-B^z_j)$$

$$+(A^x_{j,m})^2+(A^y_{j,m})^2+(A^z_{j,m})^2\ (B^x_j)^2+(B^y_j)^2+(B^z_j)^2$$

$$-2B^x_j(A^x_{j,m}T_{11}+A^y_{j,m}T_{12}+A^z_{j,m}T_{13})$$

$$-2B^y_j(A^x_{j,m}T_{21}+A^y_{j,m}T_{22}+A^z_{j,m}T_{23})$$

$$-2B^z_j(A^x_{j,m}T_{31}+A^y_{j,m}T_{32}+A^z_{j,m}T_{33}) \qquad (A5)$$

Equation (A3) is a quadratic equation in x_s. Setting $|\bar{\ell}_j|$ equal to its maximum possible value, equation (A3) can be solved to yield the value for x_s when the longest actuator has reached its full extension. Because of the motion limitations of the base no y_s, z_s, ϕ, θ, ψ combination can be obtained that gives two roots of equation (A3) of the same sign. The positive root is chosen if the x_s velocity is positive. This causes the longest actuator to be fully extended with x_s increasing in value toward the positive x_s position. Similarly the negative root is chosen if the x_s velocity is negative.

Next, from equation (A1) we determine k such that

$$|\bar{\ell}_k| \leq |\bar{\ell}_i| \quad i = 1,\ldots,6. \qquad (A6)$$

By setting $|\bar{\ell}_k|$ to its shortest possible length and solving an equation like

$$x_s^2+2G_k x+E_k = |\bar{\ell}_k|^2 \qquad (A7)$$

where G_k and E_k are similar to G_j and E_j except for k replacing j. The quadratic equation (A7) is solved and the solution for the shortest actuator is chosen in the same manner as for the longest actuator.

Hence two predicted values of the maximum available x_s excursion are obtained. One is based on the longest actuator reaching maximum extension and the other is based on the shortest actuator reaching minimum extension. These two values are compared with a specified absolute x_s limit for the system and the smallest of the three is chosen as the predicted x_s limit. In case of imaginary solutions for the quadratic equations the limit is chosen as the specified absolute limit; i.e., imaginary solutions are ignored.

The same method is used for y_s and z_s. However, no prediction is attempted for angular position limits. These limits are fixed for the system under consideration.

APPENDIX B

POSITION-VELOCITY PARABOLIC LIMITING

Consider that any given axis § of a motion base has hard constraints given by

$$\text{Position limit} = |\S| = p_\ell$$

$$\text{Velocity limit} = |\dot{\S}| = v_\ell$$

$$\text{Acceleration limit} \quad |\ddot{\S}| = a_\ell$$

Ignoring acceleration constraint, this axis of motion must be kept within $|\S| \leq p_\ell$ and $|\dot{\S}| \leq v_\ell$ which is illustrated in Figure B.1.

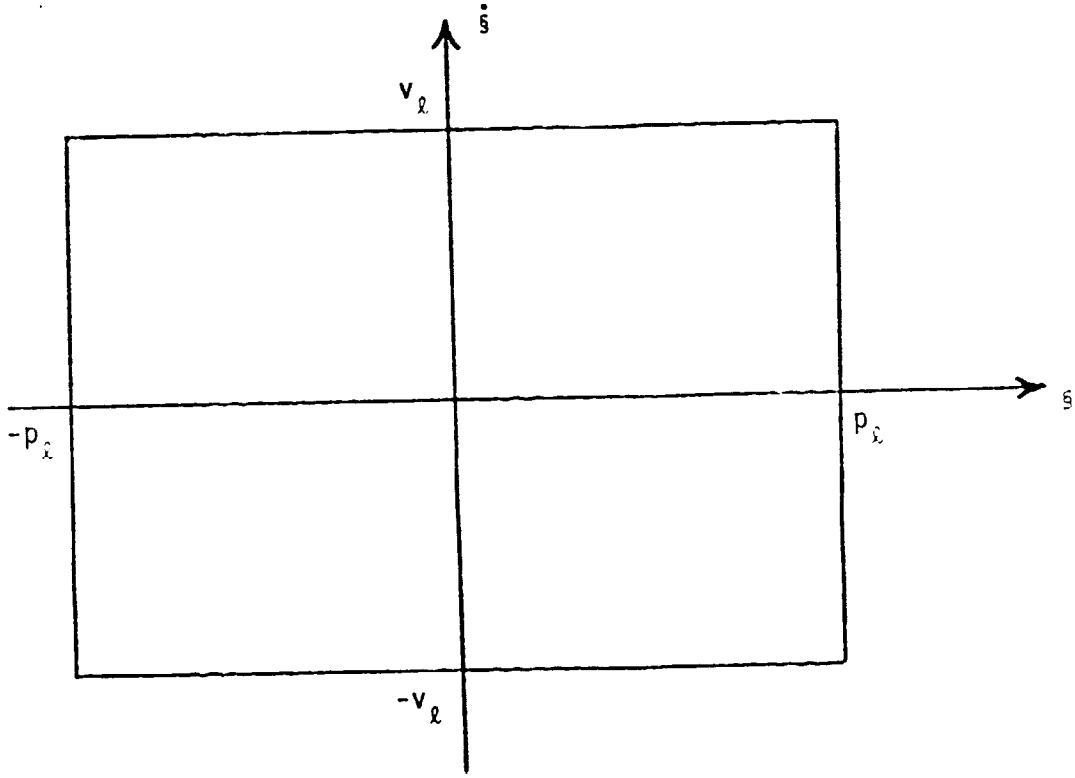

Figure B.1: Position-Velocity Limit Envelope

By definition,

$$\dot{\S} \equiv \frac{d\S}{dt} \qquad \text{(Velocity)} \tag{B1}$$

$$\ddot{\S} \equiv \frac{d}{dt}\left(\frac{d\S}{dt}\right) = \frac{d}{dt}(\dot{\S}) = \frac{d}{d\S}(\dot{\S})\cdot\frac{d\S}{dt} = \dot{\S}\frac{d\dot{\S}}{d\S} \quad \text{(Acceleration)} \tag{B2}$$

If we wish to establish the conditions for a fixed (or limiting) acceleration,

set

$$\ddot{\S} = \pm a_\ell \tag{B3}$$

Then equation (B2) yields

$$\pm a_\ell = \dot{\S}\,\frac{d\dot{\S}}{d\S} \tag{B4}$$

or

$$\pm a_\ell d\S = \dot{\S} d\dot{\S} \tag{B5}$$

integrating,

$$\pm a_\ell \int_{x_1}^{x} d\S = \int_{\dot{x}_1}^{\dot{x}} \dot{\S}\,\dot{\S} \qquad \text{where} \tag{B6}$$

$$\dot{x}_1 \equiv \dot{x}\Big|_{\S = x_1}$$

or

$$\pm a_\ell (x - x_1) = \frac{1}{2}(\dot{x}^2 - \dot{x}_1^2) \tag{B7}$$

Since we wish to have zero velocity at our position limits, the boundary conditions are

$$\left.\begin{aligned} x_1 &= \pm p_\ell \\ \dot{x}_1 &= 0 \end{aligned}\right\} \tag{B8}$$

Then equation (B7) yields

$$\pm a_{\ell}(x \mp p_{\ell}) = \frac{1}{2}\dot{x}^2 \tag{B9}$$

or

$$x = \pm \frac{1}{2a_{\ell}}\dot{x}^2 \pm p_{\ell} \tag{B10}$$

This expression contains the following four distinct possibilities

$$x - p_{\ell} = \frac{\dot{x}^2}{2a_{\ell}} \tag{B11}$$

$$x - p_{\ell} = \frac{-\dot{x}^2}{2a_{\ell}} \tag{B12}$$

$$x + p_{\ell} = \frac{\dot{x}^2}{2a_{\ell}} \tag{B13}$$

$$x + p_{\ell} = \frac{-\dot{x}^2}{2a_{\ell}} \tag{B14}$$

These four equations are represented graphically in Figure B.2. Since we are only concerned with the positions (x) within

$$-p_{\ell} \leq x \leq +p_{\ell} \quad ,$$

only (B12) and (B13) need be considered. These two equations and their graphic representation illustrate the fundamental parabolic nature of the acceleration limiting of any motion base simulator.

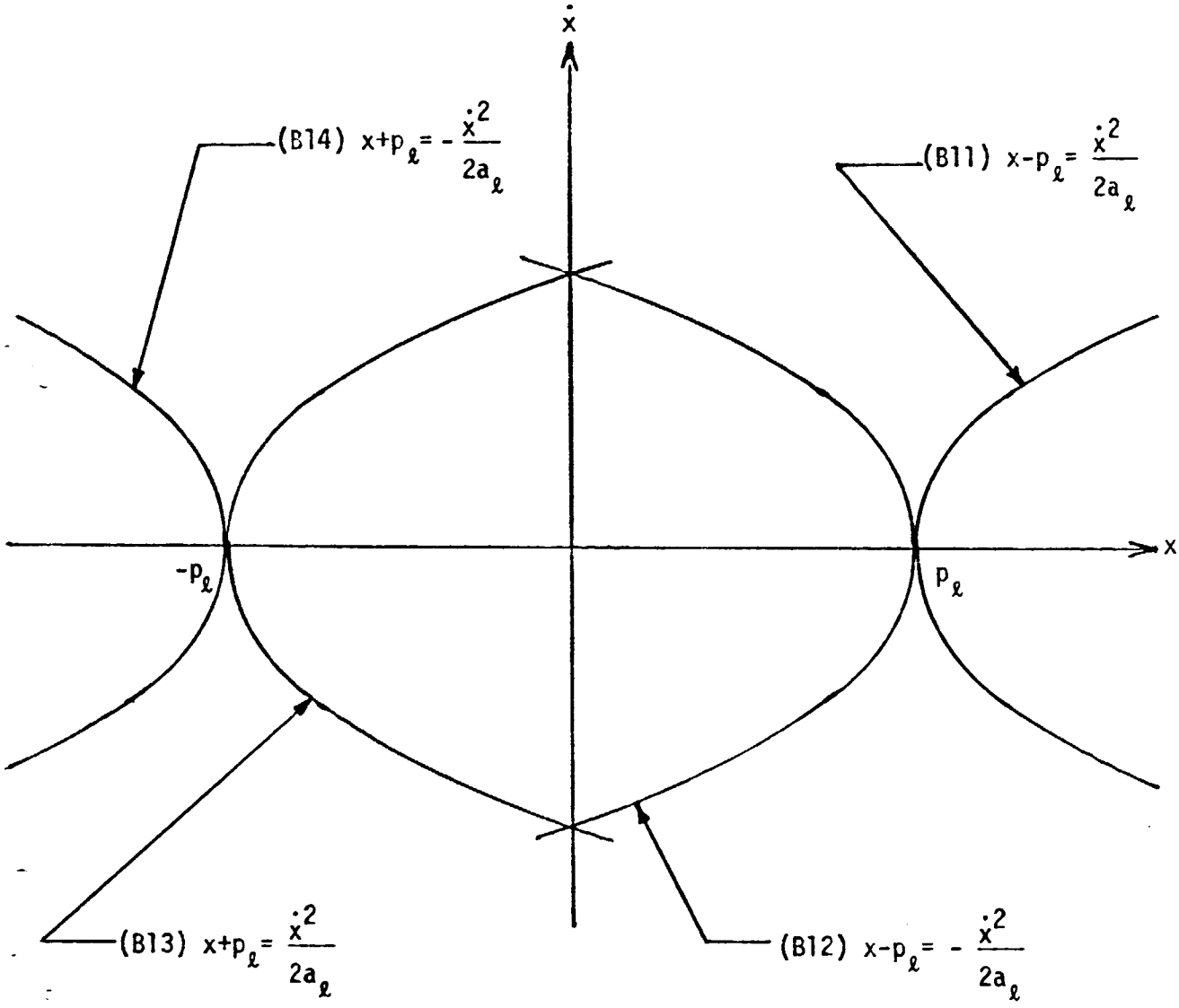

Figure B.2: Position-Velocity Phase Plane Parabolas

Superimposing the velocity limit v_ℓ on the parabolic limiting curves, the limiting envelope is as shown in Figure B.3.

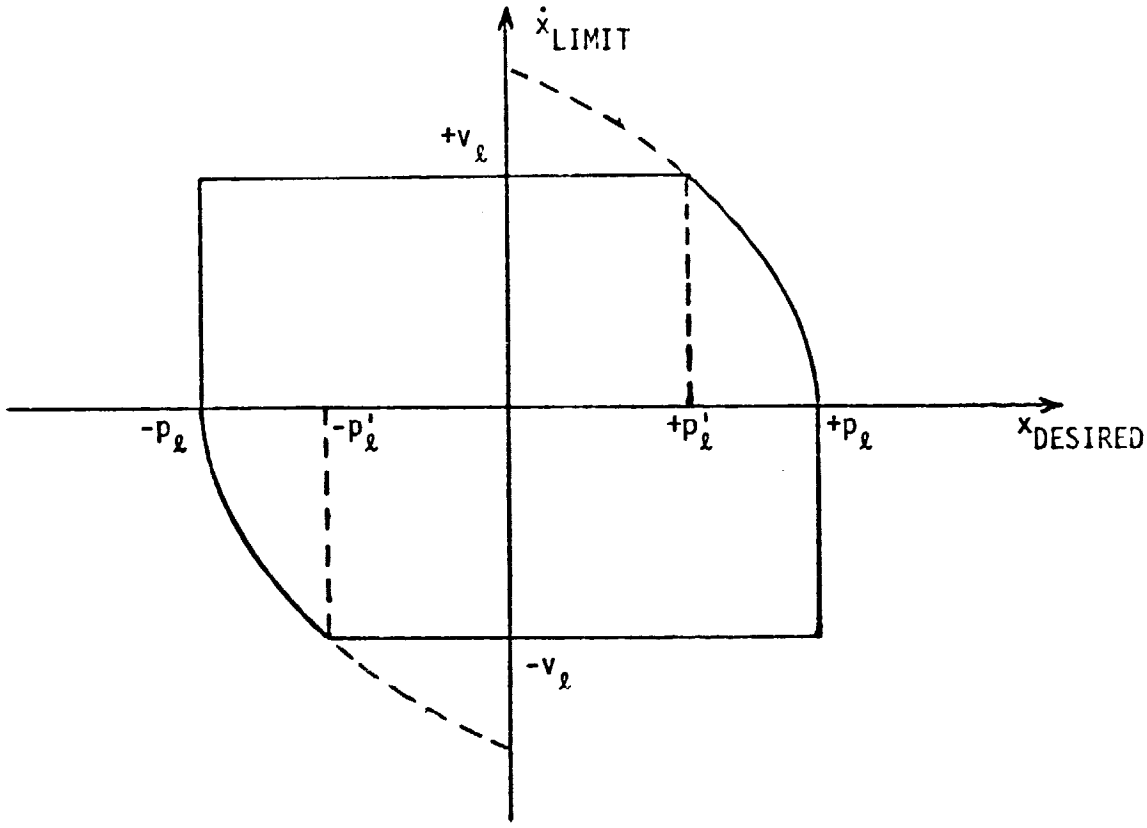

Figure B.3: Position-Velocity Limiting Envelope

The limits given by Figure B.3 can be analytically expressed as follows:

$$0 < x_{desired} < p'_\ell \quad : \quad \dot{x}_{LIMIT} = +v_\ell \tag{B15}$$

$$-p'_\ell < x_{desired} < 0 \quad : \quad \dot{x}_{LIMIT} = -v_\ell \tag{B16}$$

$$p'_\ell < x_{desired} < p_\ell \quad \& \quad (x_{current} \cdot \dot{x}_{desired}) > 0$$

$$\text{then } \dot{x}_{LIMIT} = + \sqrt{2a_\ell (p_\ell - x_{desired})} \tag{B17}$$

$$p'_\ell < x_{desired} < p_\ell \quad \& \quad (x_{current} \cdot \dot{x}_{desired}) < 0$$

$$\text{then } \dot{x}_{LIMIT} = +v_\ell \tag{B18}$$

$$-p_\ell < x_{desired} < -p'_\ell \quad \& \quad (x_{current} \cdot \dot{x}_{desired}) > 0$$

$$\text{then } \dot{x}_{LIMIT} = -\sqrt{2a_\ell (x_{desired} + p_\ell)} \tag{B19}$$

$$-p_\ell < x_{desired} < -p'_\ell \quad \& \quad (x_{current} \cdot \dot{x}_{desired}) < 0$$

$$\text{then } \dot{x}_{LIMIT} = -v_\ell \tag{B20}$$

$$\& \quad |x_{desired}| > p_\ell \quad : \quad \dot{x}_{LIMIT} = 0 \tag{B21}$$

The condition $(x_{current} \cdot \dot{x}_{desired})$ simply checks whether the simulator is moving towards the parabolic velocity limit boundary or away from it (equivalently, towards the center point or away from it).

REFERENCES

1. Schmidt, Stanley F.; and Conrad, Bjorn: Motion Drive Signals for Piloted Flight Simulators, NASA CR-1601, May 1970.

2. Conrad, Bjorn; and Schmidt, Stanley F.: A Study of Techniques for calculating Motion Drive Signals for Flight Simulators: NASA CR-114345, July 1971.

3. Zuccaro, Joseph J.: The Flight Simulator for Advanced Aircraft - A New Aeronautical Research Tool, AIAA Paper No. 70-359 (AIAA Visual and Motion Simulation Technology Conference, Cape Canaveral, Florida, March 16-18, 1970).

4. Conrad, Bjorn; Douvillier, Joseph G.; and Schmidt, Stanley F.: Washout Circuit Design for Multi-Degrees-of-Freedom Moving Base Simulators, AIAA Paper No. 73-929 (AIAA Visual and Motion Simulation Conference, Palo Alto, California, September 10-12, 1973).

5. Dieudonne, James E.; Parrish, Russel V.; and Bardusch, Richard E.: An Actuator Extension Transformation for a Motion Simulator and an Inverse Transformation Applying Newton-Raphson's Method, NASA TND-7067, November 1972.

6. Parrish, Russel V.; Dieudonne, James E.; and Martin, Dennis J., Jr.: Motion Software for A Synergistic Six-Degree-of-Freedom Motion Base, NASA TND-7350, December 1973.

Limits	Longitudinal	Lateral	Vertical	Roll	Pitch	Yaw
POSITION	±3.75 (ft.)	±40.0 (ft.)	±4.2 (ft.)	±0.698 (rad)	±0.349 (rad)	±0.436 (rad)
VELOCITY	±7.0 (ft./sec)	±12.0 (ft./sec)	±6.3 (ft./sec)	±1.76 (rad/sec)	±0.78 (rad/sec)	±0.73 (rad/sec)
ACCELERATION	±13.0 ($ft./sec^2$)	±10.0 ($ft./sec^2$)	±11.0 ($ft./sec^2$)	±6.10 (rad/sec^2)	±2.30 (rad/sec^2)	±3.03 (rad/sec^2)

Table 1: Performance capability of the Flight Simulator for Advanced Aircraft (FSAA)

Limits	Longitudinal	Lateral	Vertical	Roll	Pitch	Yaw
POSITION	±3.75 (ft.)	±4.08 (ft.)	±3.33 (ft.)	±0.38 (rad)	±0.34 (rad)	±0.43 (rad)
VELOCITY	±2.0 (ft./sec)	±2.0 (ft./sec)	±2.0 (ft./sec)	±0.35 (rad/sec)	±0.305 (rad/sec)	±0.35 (rad/sec)
ACCELERATION	±8.0 ($ft./sec^2$)	±8.0 ($ft./sec^2$)	±12.0 ($ft./sec^2$)	±0.87 (rad/sec^2)	±0.87 (rad/sec^2)	±0.87 (rad/sec^2)

Table 2: Performance capability of a typical synergistic actuator driven motion base from neutral point

		i = 1	i = 2	i = 3	i = 4	i = 5	i = 6
Moving coordinate system	A_i^x,m	6.92	-3.25	-3.68	-3.68	-3.25	6.92
	A_i^y,m	-0.25	-6.125	-5.875	5.875	6.125	0.25
	A_i^z,m	0.0	0.0	0.0	0.0	0.0	0.0
Fixed coordinate system	B_i^x	4.928	3.165	-8.093	-8.093	3.165	4.928
	B_i^y	-6.5	-7.518	-1.018	-1.018	7.518	6.5
	B_i^z	0.0	0.0	0.0	0.0	0.0	0.0

Table 3: Dimensions of a Typical Synergistic Actuator Driven Motion Base (all dimensions are in feet)

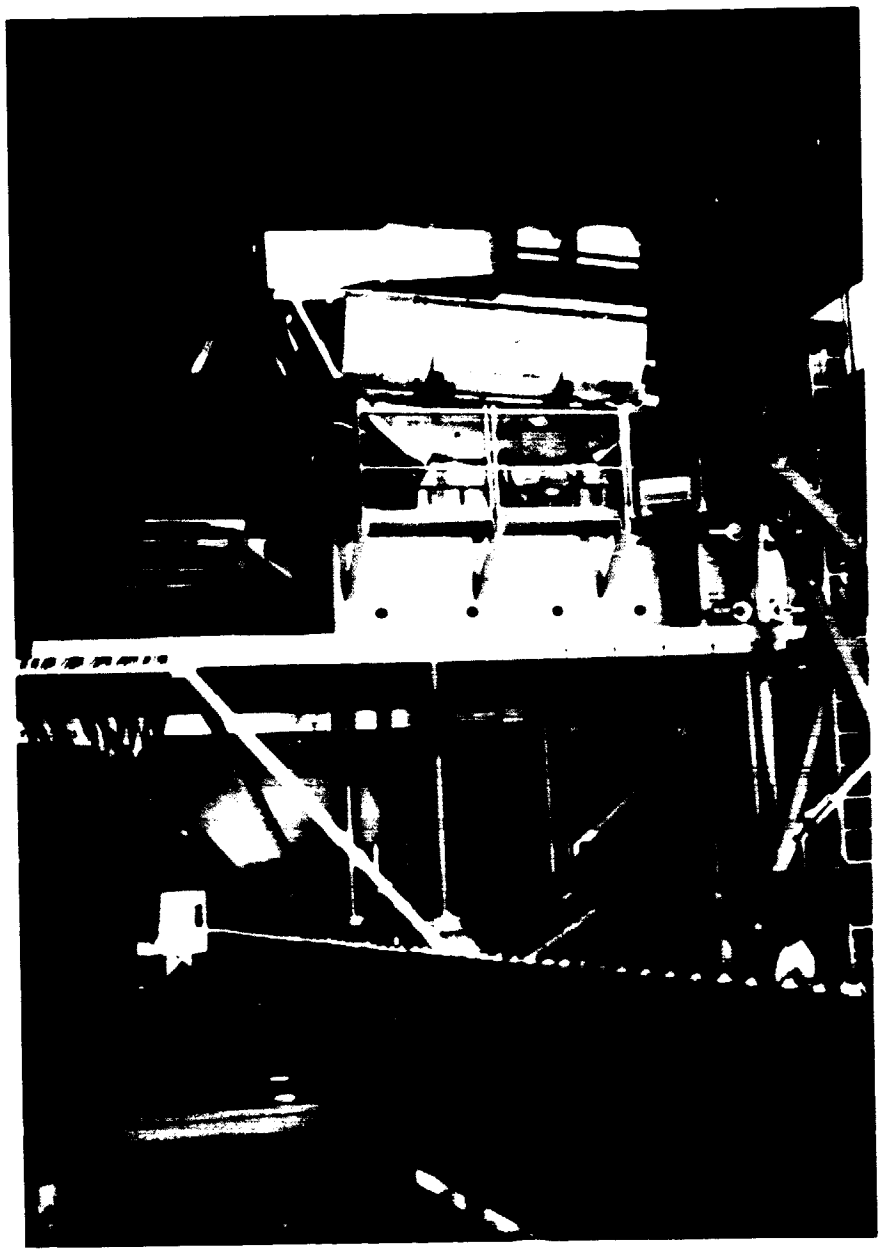

Figure 1: The FSAA Motion System [3]

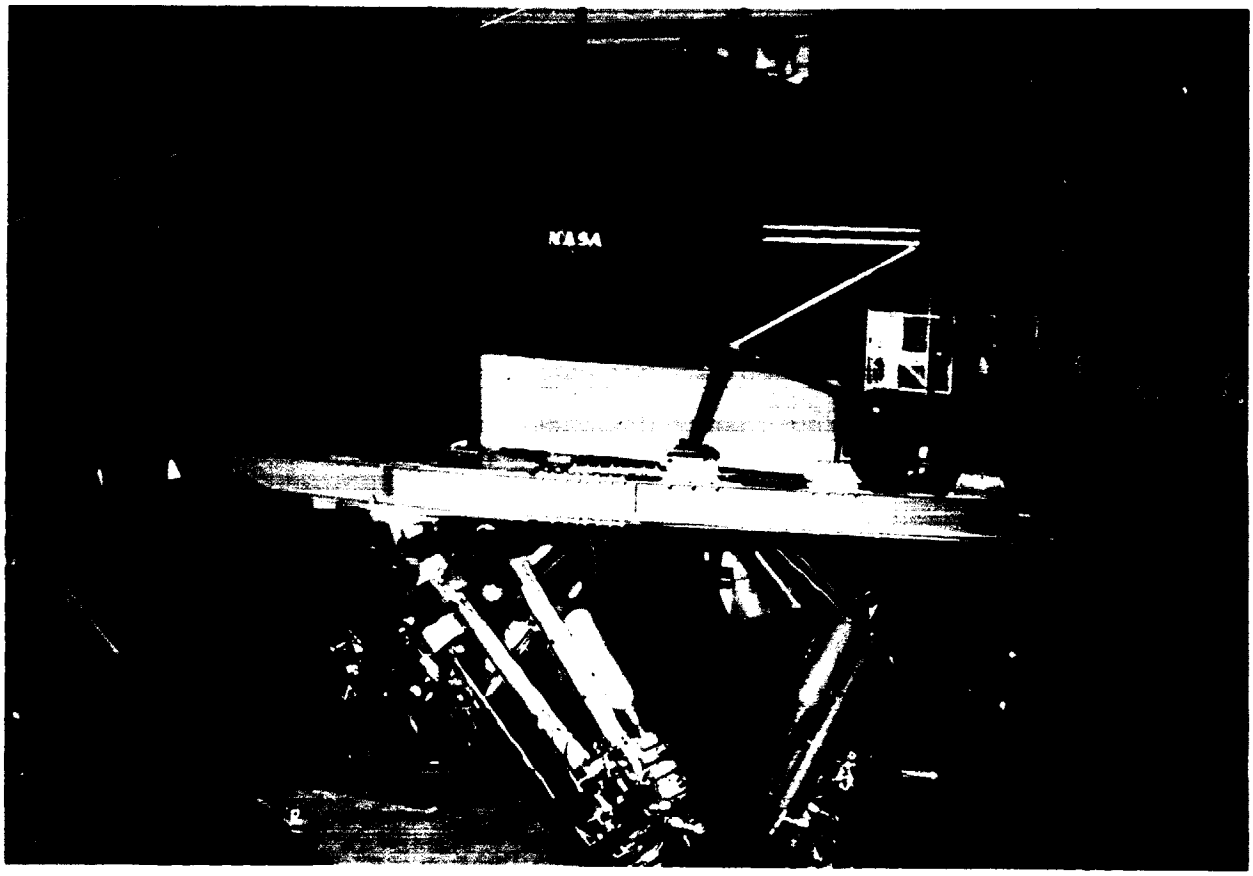

Figure 2: Langley Six-Degree-of-Freedom Motion Simulator [6]

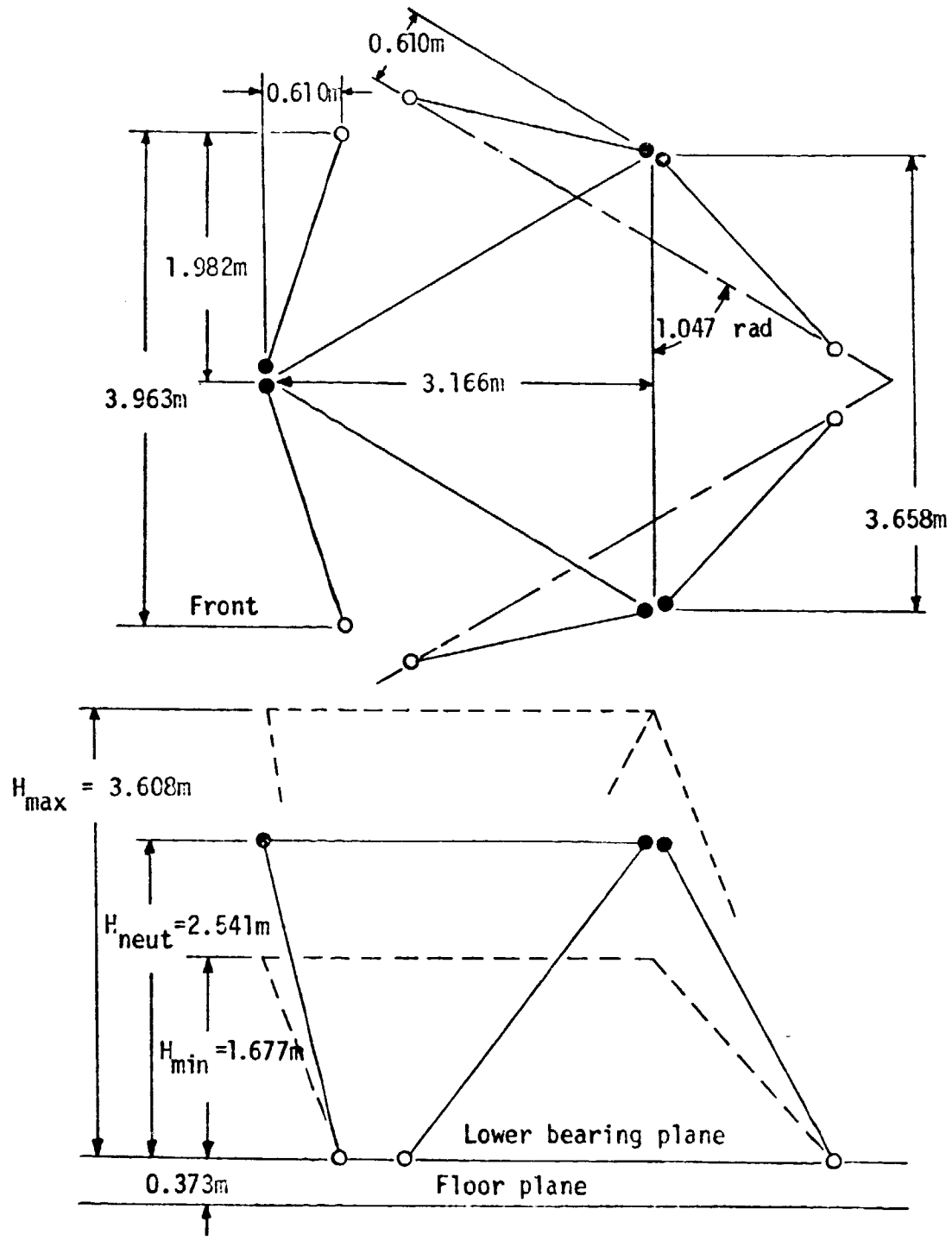

Figure 3: Motion system in neutral, settled, and raised positions. Actuator dimensions: Minimum length, 2.62m; maximum length, 4.14m. [5]

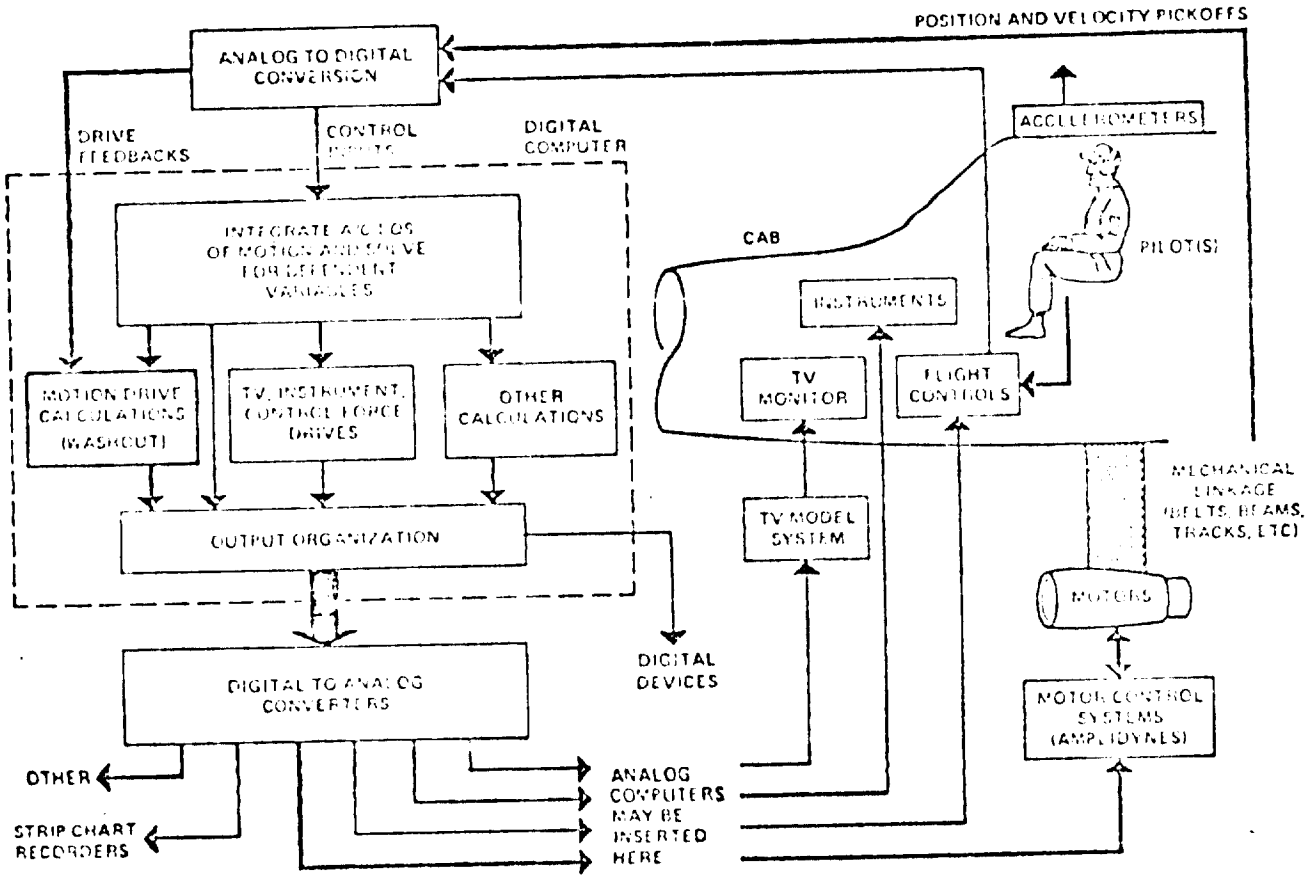

Figure 4: A Simplified Description of a Typical FSAA Simulation Configuration [4]

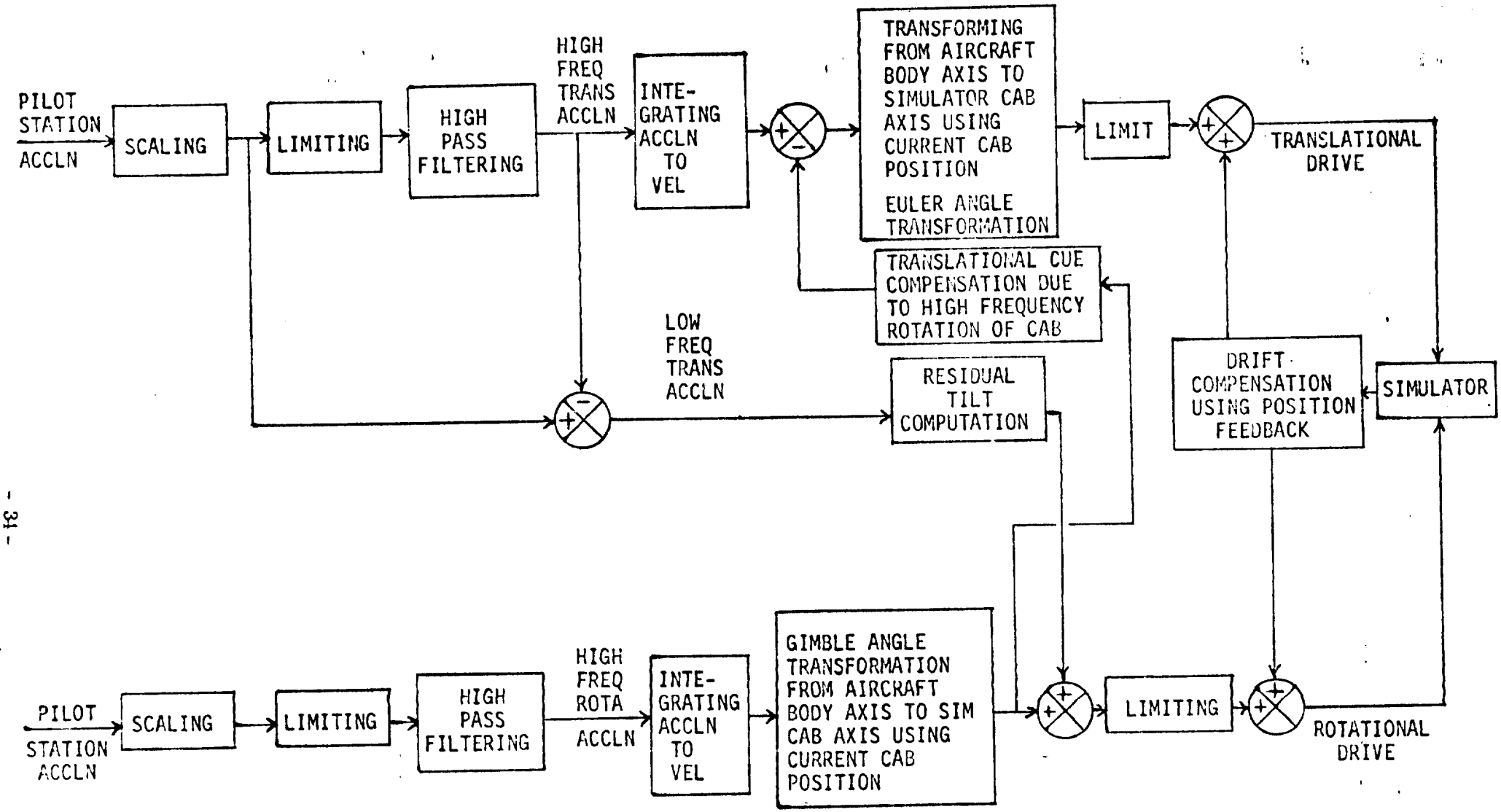

Figure 5: Motion drive logic for the FSAA for longitudinal and pitch axis or lateral and roll axis.

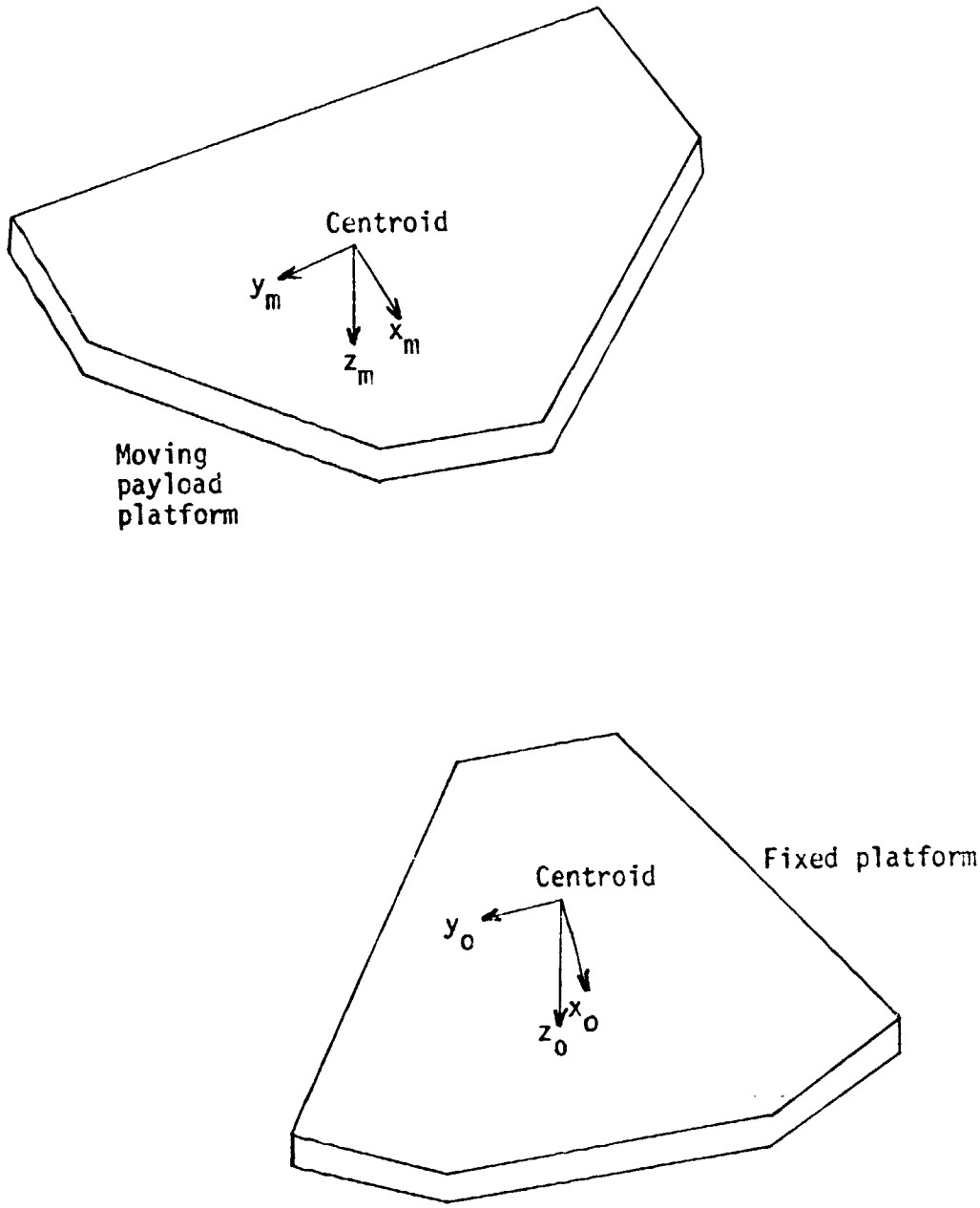

Figure 6: Coordinate Systems [5]

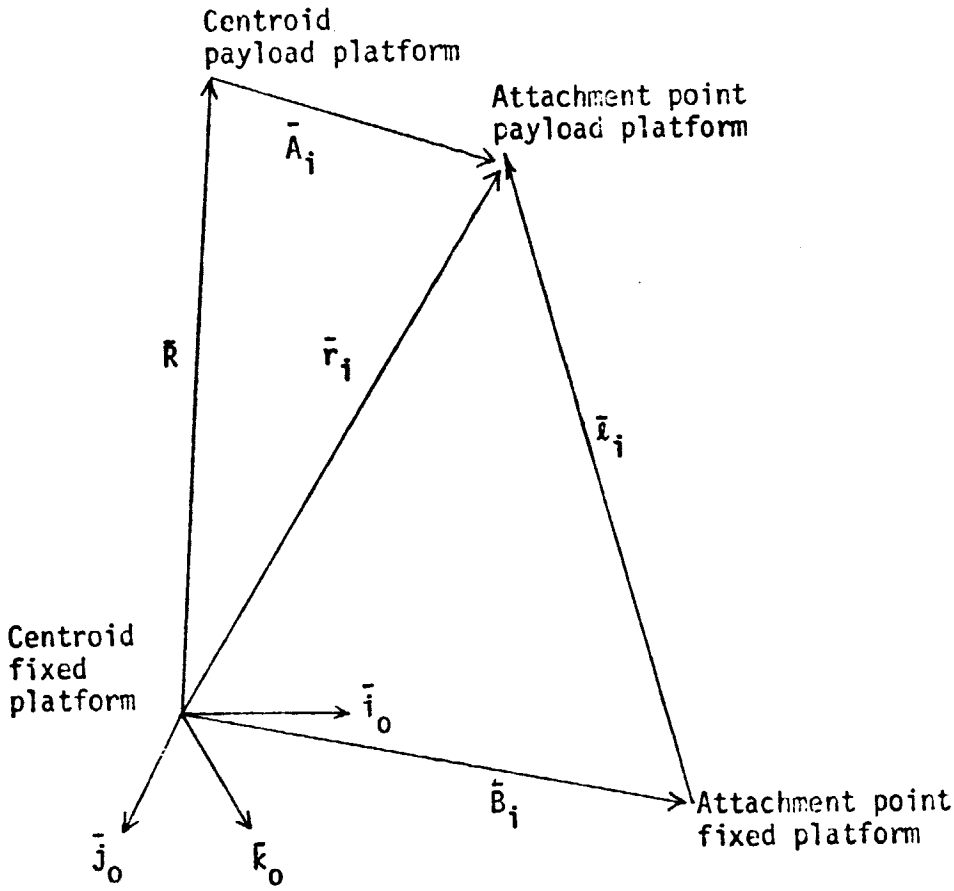

Figure 7: Vector Relationships for Actuator i [5]

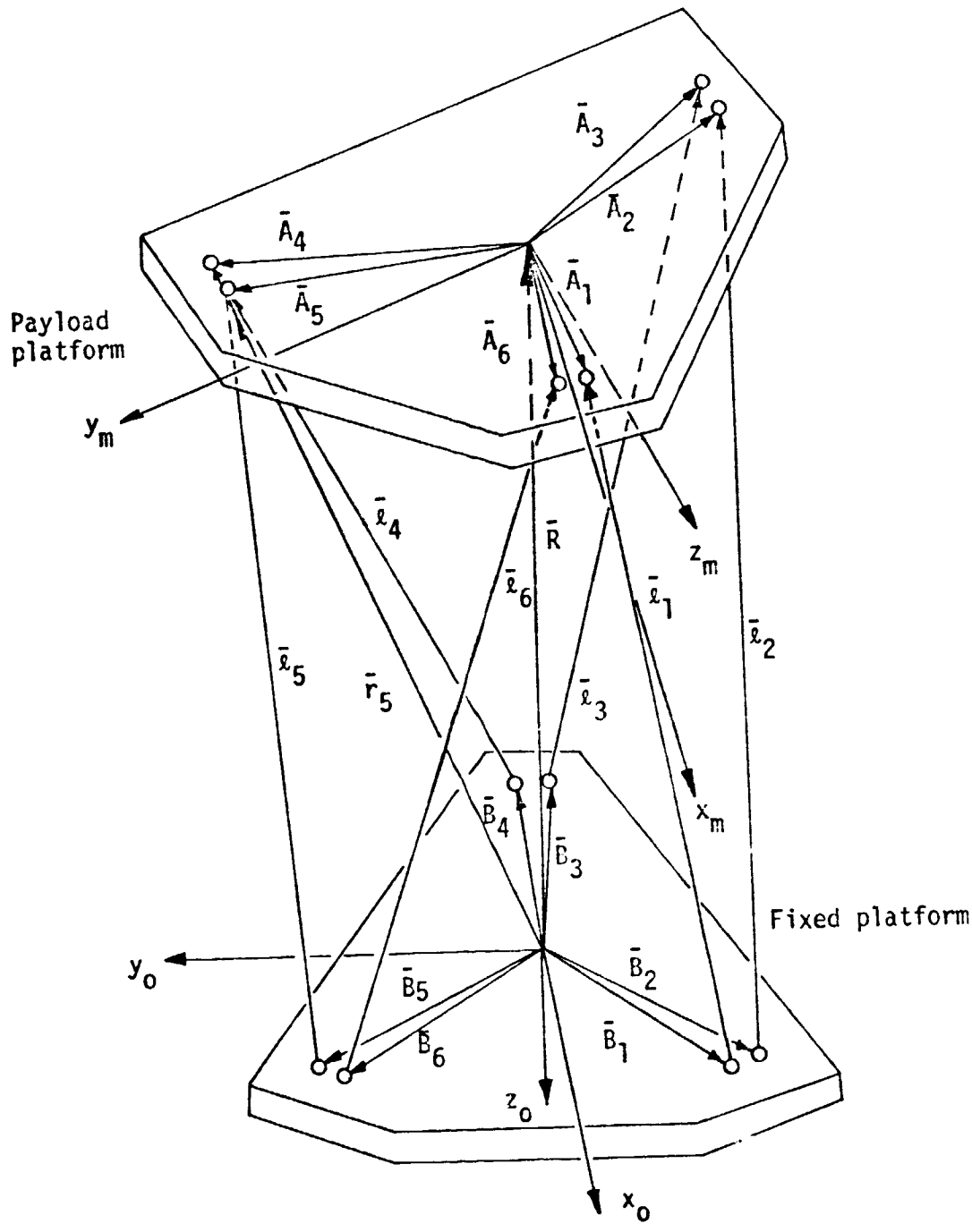

Figure 8: Arrangement of Actuators with Respect to Fixed and Moving Platform [5]

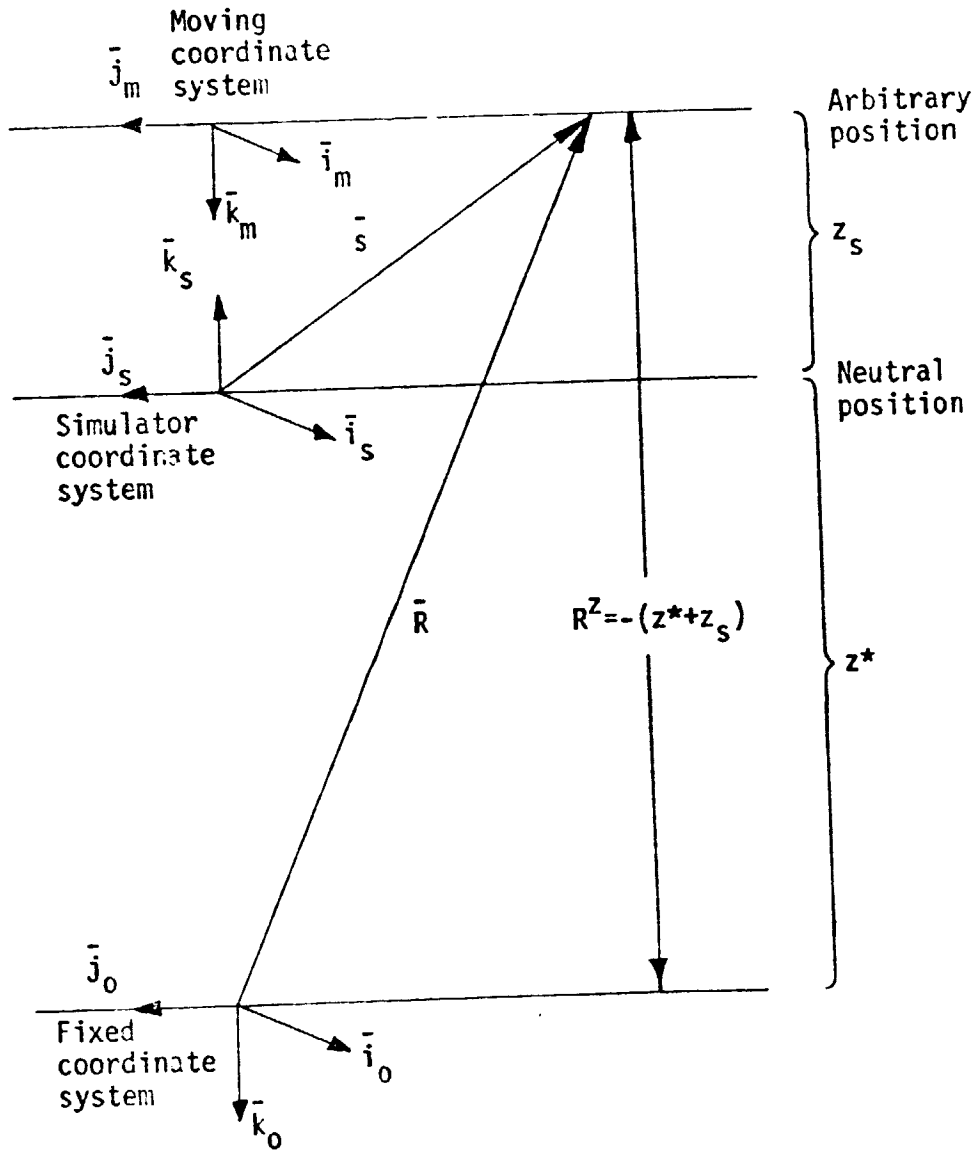

Figure 9: Relation Between Vectors $\bar{R}$ and $\bar{s}$

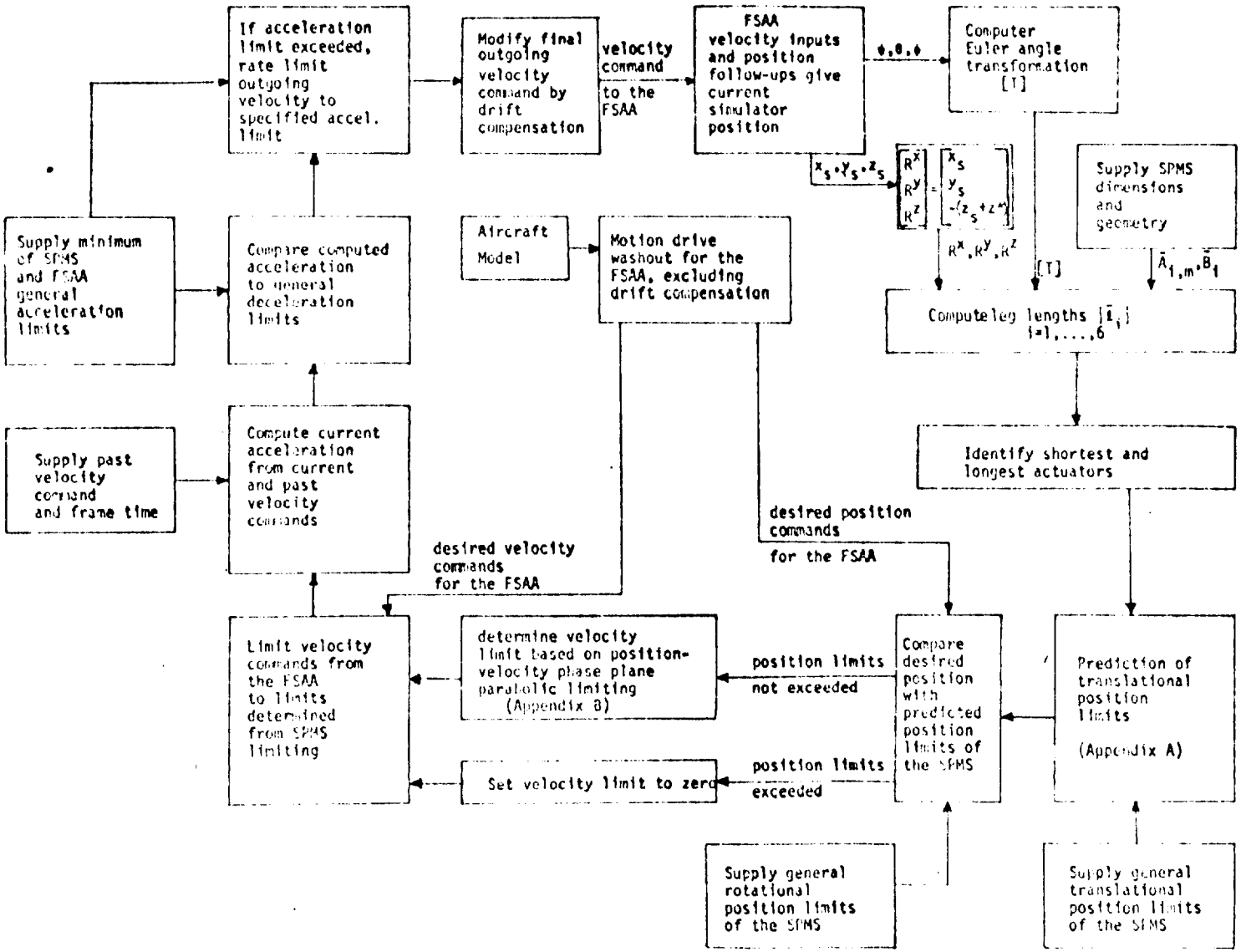

Figure 10: Motion Drive Logic for Simulating an SPMS on the FSAA

END

DATE

FILMED

OCT 4 1977